Whereas low-level activation of TRPV4 channels with synthetic agonists (e.g., 3 to 10 nM GSK) or via muscarinic receptor stimulation caused significant vasodilation ($P < 0.0001$; paired two-sample t test), higher-level activation (100 nM GSK) led to rapid global Ca^{2+} overload in ECs and oscillations of blood-vessel diameter (fig. S7 and movie S6). Notable in this context, systemic activation of TRPV4 channels by GSK causes a reduction in blood pressure and generalized circulatory failure (*14*). Collectively, these observations indicate that small numbers of EC TRPV4 channels regulate vascular physiology and suggest that pathologies characterized by blood-pressure reduction and vascular permeability increases (e.g., septic shock) may involve excessive activation of EC TRPV4 channels.

References and Notes

1. V. Hartmannsgruber *et al.*, *PLoS ONE* **2**, e827 (2007).
2. S. A. Mendoza *et al.*, *Am. J. Physiol. Heart Circ. Physiol.* **298**, H466 (2010).
3. J. Saliez *et al.*, *Circulation* **117**, 1065 (2008).
4. D. X. Zhang *et al.*, *Hypertension* **53**, 532 (2009).
5. S. Earley *et al.*, *Am. J. Physiol. Heart Circ. Physiol.* **297**, H1096 (2009).
6. I. Fleming, R. Busse, *J. Mol. Cell. Cardiol.* **31**, 5 (1999).
7. N. V. Bogatcheva, M. G. Sergeeva, S. M. Dudek, A. D. Verin, *Microvasc. Res.* **69**, 107 (2005).
8. G. Edwards, M. Félétou, A. H. Weston, *Pflugers Arch.* **459**, 863 (2010).
9. H. A. Coleman, M. Tare, H. C. Parkington, *Clin. Exp. Pharmacol. Physiol.* **31**, 641 (2004).
10. J. Ledoux *et al.*, *Proc. Natl. Acad. Sci. U.S.A.* **105**, 9627 (2008).
11. Y. N. Tallini *et al.*, *Circ. Res.* **101**, 1300 (2007).
12. Materials and methods are available as supplementary materials on *Science* Online.
13. GlaxoSmithKline compound GSK1016790A: (*N*-((1*S*)-1-{[4-((2*S*)-2-{[(2,4-dichlorophenyl)sulfonyl]amino}-3-hydroxypropanoyl)-1-piperazinyl]carbonyl}-3-methylbutyl)-1-benzothiophene-2-carboxamide; HydraBiosciences compound HC067047: (2-methyl-1-[3-{4-morpholinyl}propyl]-5-phenyl-*N*-[3-{trifluoromethyl}phenyl]-1H-pyrrole-3-carboxamide.
14. R. N. Willette *et al.*, *J. Pharmacol. Exp. Ther.* **326**, 443 (2008).
15. W. Everaerts *et al.*, *Proc. Natl. Acad. Sci. U.S.A.* **107**, 19084 (2010).
16. I. Parker, I. F. Smith, *J. Gen. Physiol.* **136**, 119 (2010).
17. W. Everaerts, B. Nilius, G. Owsianik, *Prog. Biophys. Mol. Biol.* **103**, 2 (2010).
18. S. Q. Wang, L. S. Song, E. G. Lakatta, H. Cheng, *Nature* **410**, 592 (2001).
19. R. Strotmann, M. Semtner, F. Kepura, T. D. Plant, T. Schöneberg, *PLoS ONE* **5**, e10580 (2010).
20. J. Ledoux, M. E. Werner, J. E. Brayden, M. T. Nelson, *Physiology (Bethesda)* **21**, 69 (2006).
21. K. A. Dora *et al.*, *J. Vasc. Res.* **40**, 480 (2003).
22. S. L. Sandow, C. B. Neylon, M. X. Chen, C. J. Garland, *J. Anat.* **209**, 689 (2006).

Acknowledgments: We thank HydraBiosciences for HC-067047, Neurosearch A/S for NS309, and J. E. Brayden, K. Freeman, M. Koide, L. W. Nausch, and G. C. Wellman for comments on the manuscript. This work was supported by a grant from the COBRE Program of the National Center for Research Resources funded by the NIH (2-P20-RR-016435-06), an award from the American Heart Association Founders Affiliate and the Pulmonary Hypertension Association (10POST3690006) to S.K.S, and by grants NIH GM086736 to M.I.K.; FRSQ (Junior 1)/NIA (HSFC) to J.L.; and NIH HL044455, 1P01HL095488, R37DK053832, R01HL098243, and the Totman Medical Research Trust to M.T.N. The authors have no conflicts of interest.

Supplementary Materials

www.sciencemag.org/cgi/content/full/336/6081/597/DC1
Materials and Methods
Figs. S1 to S7
Movies S1 to S6
References (*23*–*29*)

7 November 2011; accepted 16 March 2012
10.1126/science.1216283

Multidimensional Optimality of Microbial Metabolism

Robert Schuetz,[1] Nicola Zamboni,[1] Mattia Zampieri,[1] Matthias Heinemann,[1,2] Uwe Sauer[1]*

Although the network topology of metabolism is well known, understanding the principles that govern the distribution of fluxes through metabolism lags behind. Experimentally, these fluxes can be measured by ^{13}C-flux analysis, and there has been a long-standing interest in understanding this functional network operation from an evolutionary perspective. On the basis of ^{13}C-determined fluxes from nine bacteria and multi-objective optimization theory, we show that metabolism operates close to the Pareto-optimal surface of a three-dimensional space defined by competing objectives. Consistent with flux data from evolved *Escherichia coli*, we propose that flux states evolve under the trade-off between two principles: optimality under one given condition and minimal adjustment between conditions. These principles form the forces by which evolution shapes metabolic fluxes in microorganisms' environmental context.

As a network of about a thousand enzymatic reactions, metabolism fuels growth by converting nutrients into building blocks and energy, but our understanding of the principles that govern the functional distribution of fluxes through this network is limited. Experimentally, intracellular fluxes can be determined by ^{13}C-based flux analysis (*1*, *2*). Based on empirically derived optimality principles (*3*, *4*), stoichiometric models of metabolism (*3*, *4*) can predict condition-dependent flux phenotypes (*5*–*9*) as the outcome of single environment evolution (*10*, *11*). However, a concept that integrates such incidental empirical observations into a consistent framework is lacking (*12*). Although cost-benefit theory indicates that evolution in a constant environment minimizes the expression of enzymes (*10*, *13*), in reality microbes must cope with continuous environmental changes. Thus, we investigated whether the incidental objectives of metabolic operation (*5*–*10*) can be integrated into a general optimality framework that explains an organism's evolution toward particular distributions of fluxes under fluctuating conditions.

The basis of our analysis is a stoichiometric reaction model of *Escherichia coli* central metabolism (table S1) that constrains metabolic fluxes at steady state in a convex space of feasible solutions (*3*, *4*). Assuming that optimality goals are tailored to conditions and that different, eventually competing, objectives cannot be optimized simultaneously, cells face a trade-off that is described by the Pareto surface (*14*) on which each point is Pareto optimal; that is, the value of one objective can be increased only at the cost of another. To identify the axes of such a multidimensional optimality space, we computationally predicted flux distributions with 54 single objective functions and quantified the deviation to 44 reported in vivo flux distributions (fig. S1a and table S2) obtained from ^{13}C-labeling experiments (*15*–*19*) (table S3). Five of the objective functions were found to be consistent with the in vivo fluxes under some conditions: maximum adenosine triphosphate (ATP), biomass, acetate, and carbon dioxide yields and minimum sum of absolute fluxes (fig. S1a). For all possible pairs and triplets of these, we computed the Pareto surface (fig. S1b). Although no dual combination could describe all measured fluxes adequately, the combination of the two efficiency objectives, maximum ATP yield and maximum biomass yield, with the optimal resource allocation objective minimum sum of absolute fluxes achieved the highest optimality, evidenced by all 44 in vivo flux distributions being very close to the Pareto surface (Fig. 1, A and E, and figs. S1b and S2).

On the Pareto surface, the in vivo flux distributions occupied distinct regions that cluster into biologically meaningful groups (Fig. 1A). Whereas aerobic cultures of various *E. coli* strains grown with nonlimiting glucose (blue) clustered in the upper right corner, cultures in which glucose was continuously supplied at a limiting amount (green) stretched according to their growth rate diagonally between the maximum ATP and biomass yield axes. The proximity of

[1]Institute of Molecular Systems Biology, Eidgenössische Technische Hochschule (ETH) Zurich, Zurich, Switzerland. [2]Molecular Systems Biology, Groningen Biomolecular Sciences and Biotechnology Institute, University of Groningen, Groningen, Netherlands.

*To whom correspondence should be addressed. E-mail: sauer@ethz.ch

in vivo flux distributions to the Pareto surface of this three-dimensional optimality space is statistically significant because it is much closer when compared to the average distance of random steady-state flux distributions ($P < 5 \times 10^{-16}$, *t* test) (Fig. 1, B to D). Furthermore, other bacterial species also locate close to the surface (Fig. 2, A and B), and their different locations on the surface indicate that each species features a distinct flux distribution under a given condition. Thus, metabolism of wild-type bacteria appears to generally operate close to the Pareto surface of the space that defines metabolic optimality as a combination of (i) network output in the form of biomass and energy yield and (ii) resource allocation. Akin to *E. coli* (Fig. 1B), mutations can eventually shift their flux distributions away from the surface, as shown for *Bacillus subtilis* mutants with strongly altered fluxes (*20*) that locate significantly ($P < 2 \times 10^{-33}$, *t* test) below the Pareto surface (Fig. 2C), supporting our hypothesis that Pareto optimality results from evolutionary adaptation.

Why are particular flux distributions manifested in *E. coli*? For this question, we tested how Pareto optimality constrains fluxes of individual reactions. We determined the values that each reaction flux can assume in the subspace immediately below the spot on the Pareto surface where the in vivo flux distributions of a certain condition clustered together (Fig. 1E). For each of the 18 degrees of freedom (table S4) that determine all fluxes, we calculated (by exhaustive sampling) the absolute range of fluxes that each reaction can assume within the subspaces of near metabolic optimality (figs. S3 and S4). For each reaction, we thereby obtained, as a function of the distance from the Pareto surface, a flux range; that is, a variability value that defines possible fluxes at a specific optimality value (Fig. 3, A to C). For most degrees of freedom, with increasing distance from the surface the flux variability initially increases drastically before converging to stable values (Fig. 3, D to H).

All experimentally determined flux distributions were found to locate at a distance from the Pareto surface (along the *x* axes) characterized by a significant variability; for example, in aerobic batch cultures the glucose-6-phosphate dehydrogenase (Zwf) flux locates at a distance where the flux can vary from 3 to 11 mmol/g per hour at the same optimality value (Fig. 3A). The specific location is typically where a further distance increase does not further increase flux variability (Fig. 3, D to H). The almost identical position of individual flux measurements along the *y* axis indicates that the 18 tested *E. coli* wild-type strains do not exploit the full optimality-preserving variability range but rather cluster at a particular flux value (Fig. 3, A to C, and fig. S3).

So far, we found that *E. coli* operates its metabolism slightly below the Pareto surface, where it can achieve a high degree of variability in most reactions while nearly preserving

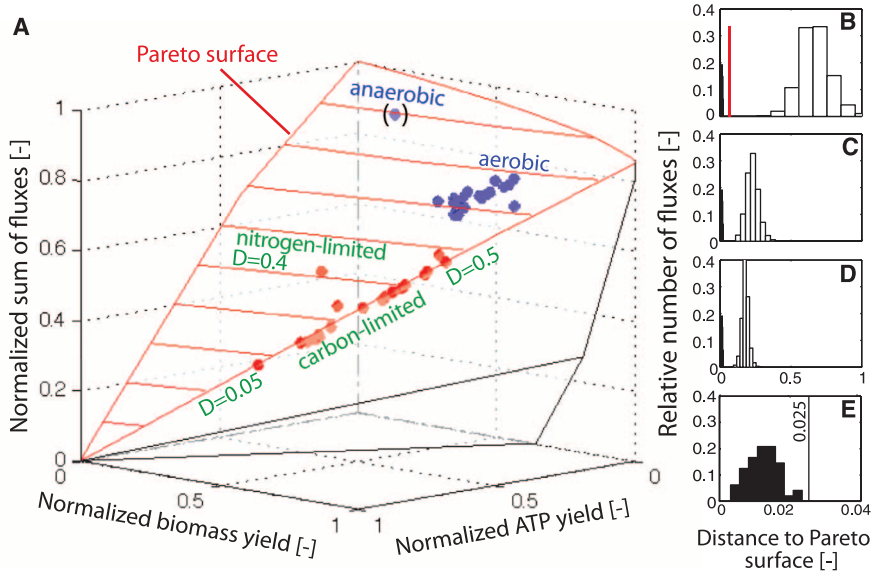

Fig. 1. (**A**) Projection of 44 ^{13}C-determined in vivo flux distributions of *E. coli* wild type into the solution space defined by three objectives. The Pareto surface is shown in red. Blue dots indicate cultures for which glucose was present in excess and green dots, continuous cultures at different dilution rates *D* (table S3) (*14*–*18*, *24*). Axes values are normalized such that the coordinates of the points on the Pareto surface range from 0 to 1, where 1 represents the theoretical minimum or maximum of an objective. Akin to the flux cone in flux balance analysis (*25*), the present space contains all mass-balanced fluxes, but the geometry is entirely different because the dimensions are objectives and not free fluxes. (**B** to **E**) Pareto surface distance of the 44 ^{13}C-determined (solid bars) and 10,000 random flux distributions (open bars) that are uniformly distributed within the full solution space (*26*). Random fluxes were chosen without imposing additional constraints (B), after elimination of futile cycles (C) and upon additionally constraining the biomass yield to at least 20% of the maximal theoretical value (D). The solid black line highlights the subspace of metabolic optimality that is relevant in vivo with a maximal distance of 0.025 units from the Pareto surface (E). Data were binned to reduce noise. The distance for the anaerobic condition is relative to its respective Pareto surface. The red bars in (B) represent the flux distribution of the *E. coli* triple mutant with deleted pyruvate formate lyase (*pfl*), lactate dehydrogenase (*ldhA*), and glucose phosphotransferase system enzyme II (*ptsG*) at CO_2 concentrations of 3, 10, and 50% (*27*).

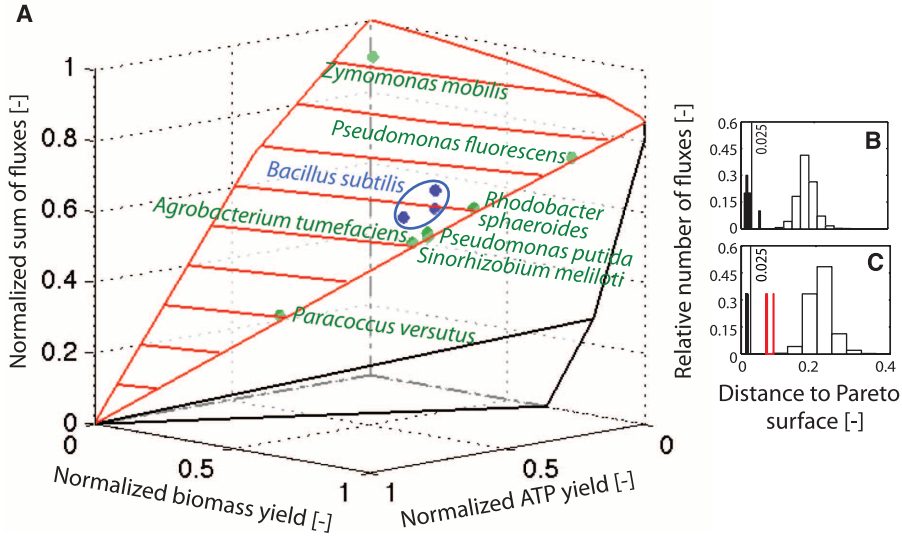

Fig. 2. (**A**) Projection of 10 ^{13}C-determined in vivo flux distributions of eight bacteria (*25*) into the metabolic optimality space of *E. coli*. The Pareto surface of *E. coli* is shown in red. The values on the axes are normalized as in Fig. 1. (**B**) Distance of the eight experimental (solid bars) and 10,000 random *E. coli* flux distributions (open bars) to each bacterium's own Pareto surface. (**C**) Distance to the Pareto surface of three *B. subtilis* wild types (solid bars); *ccpN*, *ccpN-gapB*, and *ccpN-src1 B. subtilis* mutants (*20*) (red solid bars); and 10,000 random *B. subtilis* flux distributions without futile cycles and biomass yield of at least 20% of the maximal theoretical value (open bars).

optimality. This led us to the hypothesis that additional selection criteria guide evolution toward particular flux distributions. A specific flux distribution at a certain condition might be chosen to minimize adjustment efforts to other conditions. To test this possibility, we systematically computed the average flux adjustments that would be required to switch between the five investigated environmental conditions (Fig. 4A). We calculated the range of average flux adjustments from the distances between 10,000 randomly chosen flux distributions from the optimality-preserving subspace underneath each condition (Fig. 3, A to C). We found that, although flux distributions at the Pareto surface are optimal for a given condition, they require relatively large flux adjustments to enable growth under alternative conditions (black dots in Fig. 4A). However, starting from the slightly less optimal values where the in vivo flux distributions locate, significantly smaller flux adjustments are necessary for growth under other conditions ($P < 1.4 \times 10^{-57}$, rank sum test). In the trade-off between optimality and adjustment, experimentally measured fluxes appear to minimize the adjustment efforts rather than the distance to the Pareto surface (fig. S5).

To obtain experimental evidence for minimization of flux adjustments between conditions as an evolutionary selection criterion for a flux distribution, we analyzed an *E. coli* population that was evolved for 1000 generations on alternating glucose and acetate batch cultures (*21*, *22*). The ancestor differentiated into two distinct ecotypes, that is, one exhibiting slow growth on glucose but fast to switch to acetate growth and the other with fast growth on glucose but slow to switch to acetate (*22*). Metabolically, one would expect that short switching times correspond to small flux adjustments and long switching times likewise

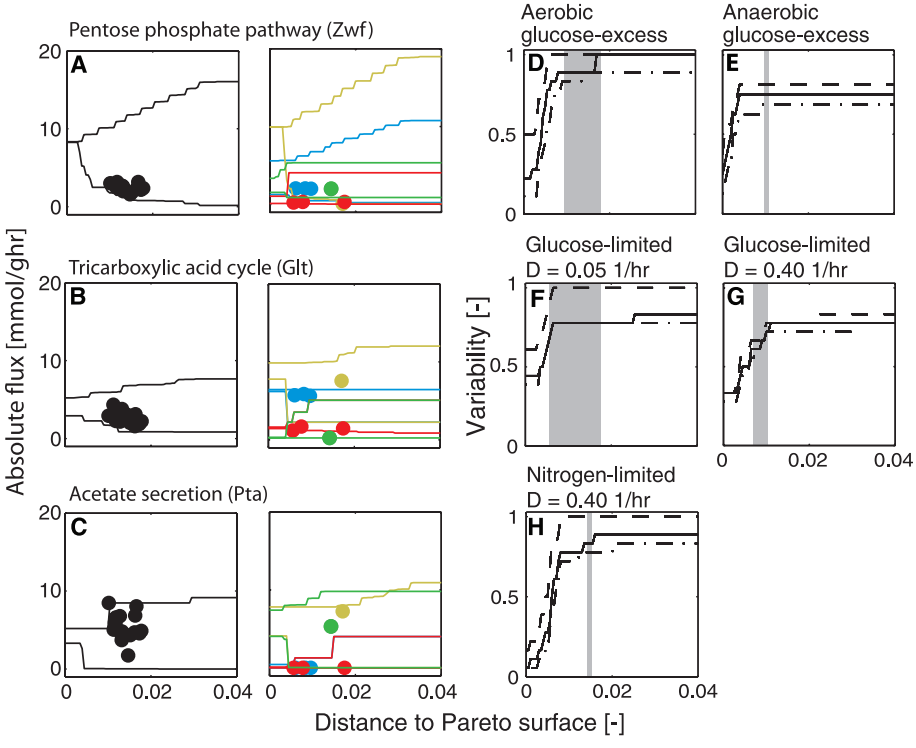

Fig. 3. Flux variability immediately below the Pareto surface for three key *E. coli* reactions. (**A** to **C**) Minimal and maximal optimal in silico fluxes (lines) and in vivo fluxes (dots) as a function of the distance to the Pareto surface in aerobic (black) and anaerobic (green) glucose batch cultures, glucose-limited continuous cultures with D = 0.09 1/hour (red) and 0.4 1/hour (light blue), and nitrogen-limited continuous cultures with D = 0.4 1/hour (dark yellow). Results for all 18 degrees of freedom are shown in figs. S3 and S4. (**D** to **H**) Variability of flux distributions as a function of their distance from the Pareto surface. Variability is defined as the fraction of degrees of freedom with a coefficient of variation (standard deviation/mean value) exceeding 10% (dashed lines), 50% (solid lines), or 80% (dashed-dotted lines) based on sampling of the metabolic optimality space. Gray areas indicate minimal and maximal distance of in vivo flux distributions.

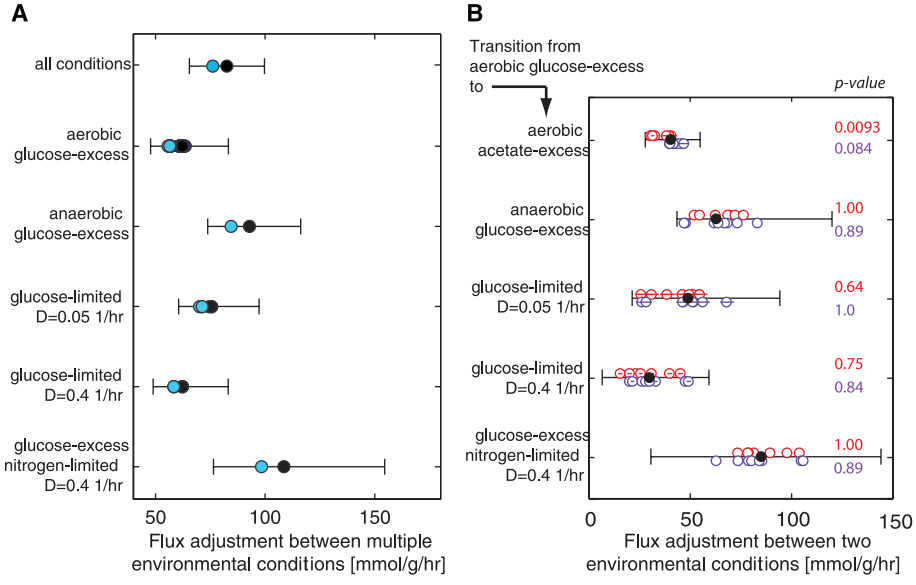

Fig. 4. Flux adjustment between multiple environmental conditions. Lines indicate the minimal and maximal average flux adjustment values based on randomly chosen flux distributions within the flexible subspace of metabolic optimality for each condition, that is, all flux distributions within a maximal distance of 0.025 units from the Pareto surface (Fig. 1E). (**A**) Average flux adjustment for switching of *E. coli* wild type from the indicated condition to any of the other four. Light blue and black dots indicate the average flux adjustment based on the in vivo realized and the hypothetical Pareto optimal flux distributions, respectively. (**B**) Flux adjustment for switching from aerobic growth on excess glucose to one of the indicated environmental conditions. Black dots indicate the unevolved strain, whereas red and green dots show evolved strains with fast or slow switching phenotypes, respectively, between aerobic growth on glucose and acetate. Average values are given where more than one experimental flux distribution was available (table S5).

correspond to large flux adjustments. Although we cannot make any predictions about the metabolism of the slow switchers, our hypothesis of minimization of flux adjustments predicts that the fast-switching strains have a flux distribution when grown on glucose that is closer to the flux distribution when grown on acetate and vice versa. Indeed, ^{13}C-labeling experiments with 15 randomly selected clones from this cyclic environment evolution (tables S5 and S6) revealed that the fast-switching ecotypes migrated toward Pareto optimality and an in-between flux distribution with, for example, higher tricarboxylic acid cycle fluxes on glucose (fig. S6) that lead to significantly ($P < 0.009$) reduced flux adjustments between growth on glucose and acetate (Fig. 4B and fig. S7). The slow switchers, in contrast, exhibited higher flux adjustment values than the ancestor. Consistent with our hypothesis, the flux adjustments from glucose batch growth to any other (not selected for) environmental condition scatter around the ancestor with no significant difference between the two ecotypes (Fig. 4B). Thus, within the optimality-preserving variability at one condition, evolution favors flux distributions that minimize adjustments to other environmental conditions.

The principles of variable, near-optimal metabolism and minimal flux adjustment suffice to explain all investigated flux distributions. The range of investigated bacteria and conditions suggests that these principles are prevalent. In contrast to the previously described adaptive prediction, in which regulation patterns evolved that anticipated sequential environmental changes (*23*), the adaptive property of minimal flux adjustment is not restricted to the temporal order of occurring environments. Instead, minimal flux adjustment represents more generally an optimal starting point for growth under multiple conditions, presumably reflecting an organism's natural habitat(s). An organism cannot be optimally adapted to all possible conditions, but the evolutionary benefit of an ideal starting point will be important for microbes that are not highly specialized to particular nutritional conditions. By this trade-off between (near) optimality under a given condition and minimal adjustment to alternative conditions, we provide a consistent theoretical framework to decipher optimality-based forces that shape metabolic fluxes in a microorganism's environmental context.

References and Notes

1. U. Sauer, *Mol. Syst. Biol.* **2**, 62 (2006).
2. N. Zamboni, S.-M. Fendt, M. Rühl, U. Sauer, *Nat. Protoc.* **4**, 878 (2009).
3. M. A. Oberhardt, B. O. Palsson, J. A. Papin, *Mol. Syst. Biol.* **5**, 320 (2009).
4. A. M. Feist, M. J. Herrgård, I. Thiele, J. L. Reed, B. O. Palsson, *Nat. Rev. Microbiol.* **7**, 129 (2009).
5. R. Schuetz, L. Kuepfer, U. Sauer, *Mol. Syst. Biol.* **3**, 119 (2007).
6. A. P. Burgard, C. D. Maranas, *Biotechnol. Bioeng.* **82**, 670 (2003).
7. H.-G. Holzhütter, *Eur. J. Biochem.* **271**, 2905 (2004).
8. D. Segrè, D. Vitkup, G. M. Church, *Proc. Natl. Acad. Sci. U.S.A.* **99**, 15112 (2002).
9. T. Shlomi, O. Berkman, E. Ruppin, *Proc. Natl. Acad. Sci. U.S.A.* **102**, 7695 (2005).
10. N. E. Lewis *et al.*, *Mol. Syst. Biol.* **6**, 390 (2010).
11. R. U. Ibarra, J. S. Edwards, B. O. Palsson, *Nature* **420**, 186 (2002).
12. A. M. Feist, B. O. Palsson, *Curr. Opin. Microbiol.* **13**, 344 (2010).
13. E. Dekel, U. Alon, *Nature* **436**, 588 (2005).
14. D. Nagrath *et al.*, *Ann. Biomed. Eng.* **35**, 863 (2007).
15. A. Perrenoud, U. Sauer, *J. Bacteriol.* **187**, 3171 (2005).
16. M. Emmerling *et al.*, *J. Bacteriol.* **184**, 152 (2002).
17. N. Ishii *et al.*, *Science* **316**, 593 (2007); 10.1126/science.1132067.
18. A. Nanchen, A. Schicker, U. Sauer, *Appl. Environ. Microbiol.* **72**, 1164 (2006).
19. E. Fischer, U. Sauer, *Eur. J. Biochem.* **270**, 880 (2003).
20. S. Tännler *et al.*, *J. Bacteriol.* **190**, 6178 (2008).
21. C. C. Spencer, J. Tyerman, M. Bertrand, M. Doebeli, *Proc. Natl. Acad. Sci. U.S.A.* **105**, 1585 (2008).
22. C. C. Spencer, M. Bertrand, M. Travisano, M. Doebeli, *PLoS Genet.* **3**, e15 (2007).
23. A. Mitchell *et al.*, *Nature* **460**, 220 (2009).
24. T. Fuhrer, E. Fischer, U. Sauer, *J. Bacteriol.* **187**, 1581 (2005).
25. N. D. Price, J. L. Reed, B. O. Palsson, *Nat. Rev. Microbiol.* **2**, 886 (2004).
26. D. Kaufman, R. Smith, *Oper. Res.* **46**, 84 (1998).
27. S. Lu, M. A. Eiteman, E. Altman, *J. Biotechnol.* **143**, 213 (2009).

Acknowledgments: R.S. is in the Life Science Zurich Ph.D. program on Systems Physiology and Metabolic Diseases, Zurich, Switzerland. We thank M. Doebeli for the mutants, E. Michlig for flux analysis, J. Banga for initial discussion on Pareto optimality, and V. Chubukov for proofreading. We acknowledge financial support via an ETH grant to U.S. Data and model described in this paper are presented in the supplementary materials.

Supplementary Materials

www.sciencemag.org/cgi/content/full/336/6081/601/DC1
Materials and Methods
Supplementary Text
Figs. S1 to S9
Tables S1 to S6
References (*28*–*38*)

21 November 2011; accepted 16 March 2012
10.1126/science.1216882

Radio-Wave Heating of Iron Oxide Nanoparticles Can Regulate Plasma Glucose in Mice

Sarah A. Stanley,[1] Jennifer E. Gagner,[2] Shadi Damanpour,[1] Mitsukuni Yoshida,[3] Jonathan S. Dordick,[4] Jeffrey M. Friedman[1,5]*

Medical applications of nanotechnology typically focus on drug delivery and biosensors. Here, we combine nanotechnology and bioengineering to demonstrate that nanoparticles can be used to remotely regulate protein production in vivo. We decorated a modified temperature-sensitive channel, TRPV1, with antibody-coated iron oxide nanoparticles that are heated in a low-frequency magnetic field. When local temperature rises, TRPV1 gates calcium to stimulate synthesis and release of bioengineered insulin driven by a Ca^{2+}-sensitive promoter. Studying tumor xenografts expressing the bioengineered insulin gene, we show that exposure to radio waves stimulates insulin release from the tumors and lowers blood glucose in mice. We further show that cells can be engineered to synthesize genetically encoded ferritin nanoparticles and inducibly release insulin. These approaches provide a platform for using nanotechnology to activate cells.

Remote activation of specific cells to trigger gene expression and peptide release in vivo could provide a useful research tool and, in time, potentially provide a means for regulated expression of proteins in clinical settings. Cell activation by direct stimulation with electrodes (*1*) is limited by nonspecific and variable activation, the need for permanent implants, and potential tissue damage (*2*, *3*). Ion channels, such as channelrhodopsin, regulate intracellular ions and cell activity (*4*) with anatomical specificity and temporal control, but, because light waves do not penetrate tissue, implanted devices are required. In contrast, low and medium radio frequencies (RFs) can penetrate deep tissues with minimal energy absorption (*5*, *6*). Unlike tissue, metal nanoparticles absorb energy and heat in response to RF (*7*, *8*). This heating, which depends on particle composition and size and RF field strength, (*9*) can be converted into a cellular signal by using a temperature-sensitive channel to allow ion entry. Targeting of nanoparticles can be achieved by coating with specific antibodies (*10*, *11*) to induce cell-specific, cell membrane

[1]Laboratory of Molecular Genetics, Rockefeller University, New York, NY 10065, USA. [2]Department of Materials Science and Engineering, Rensselaer Nanotechnology Center, Rensselaer Polytechnic Institute, Troy, NY 12180, USA. [3]Elizabeth and Vincent Meyer Laboratory of Systems Cancer Biology, Rockefeller University, New York, NY 10065, USA. [4]Department of Chemical and Biological Engineering, Department of Biology, Center for Biotechnology and Interdisciplinary Studies, Rensselaer Polytechnic Institute, Troy, NY 12180, USA. [5]Howard Hughes Medical Institute, New York, NY 10065, USA.

*To whom correspondence should be addressed. E-mail: friedj@mail.rockefeller.edu